applied sciences

MDPI

Article

# Research on the Modeling, Control, and Calibration Technology of a Tracked Vehicle Load Simulation Test Bench

**Haoliang Lv [1,2], Xiaojun Zhou [1,2,*], Chenglong Yang [1,2], Zhe Wang [1,2] and Yimeng Fu [1,2]**

1 The State Key Lab of Fluid Power and Mechatronic Systems, College of Mechanical Engineering, Zhejiang University, Hangzhou 310027, China; lhl801@zju.edu.cn (H.L.); yclzju@163.com (C.Y.); wzhe@zju.edu.cn (Z.W.); zjume_Fuyimeng@zju.edu.cn (Y.F.)

2 Key Laboratory of Advanced Manufacturing Technology of Zhejiang Province, College of Mechanical Engineering, Zhejiang University, Hangzhou 310027, China

* Correspondence: cmeesky@163.com; Tel.: +86-1806-986-4060

Received: 27 May 2019; Accepted: 20 June 2019; Published: 22 June 2019

**Featured Application: The device mentioned in this paper can be used for the road simulation test of a power system of a heavy haul vehicle. The method mentioned in this paper can be used to model, control, and calibrate the vehicle load simulator.**

**Abstract:** The load simulation test bench plays an important role in tracked vehicle development. The stability and accuracy of the system have a vital impact on the experimental results. To accurately reproduce the power performance of a tracked vehicle on the test platform, this paper aims to investigate the model, control, and calibration method of the test bench. Firstly, the dynamic model of a tracked vehicle under complex driving conditions is analyzed and established, which takes driving torque as the input and driving wheel speed as the output. Then, considering the uncertainties and disturbances in the system model, a 2-degree-of-freedom (2-DOF) control method combined with a disturbance observer is proposed to solve the stability problem of the system. Furthermore, in order to investigate the accuracy of the simulation on the test bed, a method of calibrating the system by a flywheel set with standard inertia is proposed. In the calibration process, the influence of the system resistance torque and the original mechanical inertia on the results is considered, and the response time of the inertia simulation is analyzed in both a steady and dynamic state. Finally, the load simulation test is carried out with the corrected system. The test results show that the system has a high load simulation accuracy under various load simulation tests.

**Keywords:** tracked vehicle; load simulator; test bench; uncertainty and disturbance; control method; calibration

## 1. Introduction

Tracked vehicles are widely used in agriculture, weapons, and engineering construction because of their superior performance under complex conditions. The load simulation technology of a tracked vehicle is rapidly evolving because it can provide a convenient, effective, and lifelike test environment [1–3]. By modifying different parameters on the test bench, the power output, emission performance, and braking performance of the vehicle under different temperature, humidity, and ground conditions can be tested. Additionally, only when the body inertia and ground load simulated by the loading system are consistent with the real situation can the load simulation research test be meaningful [4–7]. At present, in order to overcome the problem that the traditional mechanical simulation method has a narrow simulation range and cannot achieve stepless simulation, most

researchers use the method of an electric motor to simulate mechanical inertia (hereinafter referred to as electrical inertia) [8,9].

In order to realize vehicle load simulation, it is necessary to model the tested vehicle and design the control system of the bench in turn. The establishment of an accurate dynamic model is the premise to achieve accurate load simulation. When the traditional method is used to establish the dynamic model of a wheeled vehicle, the equivalent mass of translational motion is calculated by estimating the coefficient of the rotating parts of the vehicle, such as wheels and transmission systems, and the equivalent inertia of the output shaft is then obtained [10,11]. For tracked vehicle modeling, the kinetic energy of its rotating parts and the slip rate between the vehicle and the ground are basically neglected. Because the ratio of the mass of rotating parts to the total mass of wheeled vehicles is small, the estimation error of equivalent mass is small. The revolving parts of tracked vehicles include those that account for a larger proportion of the vehicle weight, and some of them weigh up to a quarter of the vehicle weight. If the same calculation method is used as that of a wheeled vehicle, the larger error will be substituted. Therefore, the equivalent inertia of a tracked vehicle is deduced. The equivalent inertia of its rotating parts, such as the track and wheel, should be independently modeled and calculated respectively.

The design goal of the control system is to achieve accurate load simulation. At present, there are many methods that can be employed to realize load simulation. Reference [12] introduces an inverse dynamic method, which uses the inverse dynamic model of the tested vehicle and test-bed system to get the simulated load. The motor controls the torque according to the load. This method is simple and commonly used. However, the inverse dynamics model is usually irregular, so it contains differential terms, which will generate noise and lead to system instability. Reference [13,14] proposes a speed tracking method, which introduces a torque sensor to measure the output torque of the tested system, and then obtains the system speed according to the dynamic model of the system, and uses the motor to follow the target speed. This method avoids inverse dynamics. Akpolat compares the two methods by simulation, and points out that the speed tracking method is suitable for the control scheme of a large non-linear load. Reference [15,16] conducts a further investigation based on the study of the inverse dynamic method and speed tracking method. The system control framework is built by using a PI controller and PI estimator respectively, which aims to solve some of the drawbacks of the speed tracking method, such as the sensitivity to parameter variation, which makes it less accurate for the emulating of high-speed and high-power loads. Relevant tests on electrical vehicles and a non-linear pendulum are carried out, and good results are obtained.

When the motor system and its accessories are used as inertia simulation equipment, the additional resistance of the equipment is always changing due to the influence of the friction coefficient and environment (including temperature, humidity, lubricant cleanliness, etc.). In addition, the thermal change of the actuator will bring additional torque. These changes will change the transfer function of the system during operation, resulting in a poor robustness of the system [17,18].

In Reference [19,20], non-linear factors of the test bench are analyzed, and the effects of elasticity and backlash nonlinearity on the system performance are fully considered. Aiming at the high-order, non-linear, and multi-variable characteristics of the test-bed system, control methods suitable for each test-bed are proposed. It avoids the complex algorithm of closed-loop speed compensation and reduces the influence of inaccurate model parameters on the control accuracy of the simulation system. Literature [21] discusses the effects of inertia and the viscous friction coefficient of the load simulation system on system speed control and load simulation. The influence of inertia and the viscous friction coefficient on the test bench is analyzed through theoretical derivation and an experiment.

Because of the hysteresis of motor control, the errors caused by this change can hardly be eliminated. At the same time, in the motor control part, the instantaneous forward and backward electrodynamic force of the equipment and the simplification of the system control from higher order to lower order will also bring errors to the system control [22]. Therefore, no matter what control

method is adopted, the error of inertia simulation is always unavoidable. In this regard, it is very important to calibrate the load simulation system.

At present, the calibration work of the vehicle load simulation system is less abundant, while the calibration methods of other load simulation systems can be used for reference. Reference [23] showcases the calibration work for a piezoelectric thrust dynamometer for small thrust liquid pulsed rocket engines. The calibration work is divided into static and dynamic parts. The static part calibrates the static output of the thrust dynamometer using high-precision piezoelectric sensors. The dynamic calibration part uses a standard steel ball to rotate at a certain frequency to determine the natural frequency of the pulse thrust dynamometer. Reference [24] presents a measurement method for the dynamic calibration of dynamometers after static calibration. However, under static and dynamic conditions, the friction loss of bearings varies, depending on the speed and torque. Therefore, the accuracy of calibration is not evaluated in this paper. Reference [25] has calibrated a force–moment measurement system for wheel–rail contact mechanics in roller rigs. In this paper, the quasi-static calibration of the measurement system is carried out by using mass blocks, and the quasi-static calibration results are fitted for dynamic measurement.

Although many researchers have conducted a lot of work on the simulation of electrical inertia, the existing methods at present are limited to the calibration of the accuracy of a single sensor, and there is no system-level calibration method for a large inertia load simulator [26–30].

According to the electrical simulation theory of mechanical inertia, a dynamic model of a tracked vehicle under actual road conditions is established, and the control model is established considering the uncertainties and disturbances of the system. By adopting the method of using standard flywheel sets to calibrate electrical inertia, a calibration method of electrical inertia simulation accuracy for various working conditions is established, and the simulation accuracy and response time under the control strategy are calibrated.

## 2. Principle and Modeling

The principle of the load simulation of a vehicle driving system is to reproduce the load equivalently to the test bench. In short, the driving resistance is simulated by a motor or other equipment and applied to the driving wheel of the tested vehicle. According to this principle, the structure of the load simulation test bench is designed as shown in Figure 1. The system consists of two parts: the load simulation system and the tested vehicle. The tested vehicle is fixed in the environment chamber, which can simulate the environment during the test, such as temperature, humidity, salinity, and so on. The driving wheels on both sides of the tested vehicle are connected to the load simulation system through the transmission shaft. The load simulation system consists of an electric motor, reducer, transmission shaft, torque meter, and encoder. In order to adapt to the height of different vehicles, the universal transmission shaft is used between the output end of the gearbox and the vehicle being tested. Under this structure, when starting the vehicle and stepping the throttle down, the current speed and torque are obtained by the encoder and torque meter. By combining the torque signal with the vehicle dynamic model, the target speed of the driving wheel can be calculated. Driving the motor to track the speed, the driving wheel of the tested vehicle can be subjected to the same load as actual road driving.

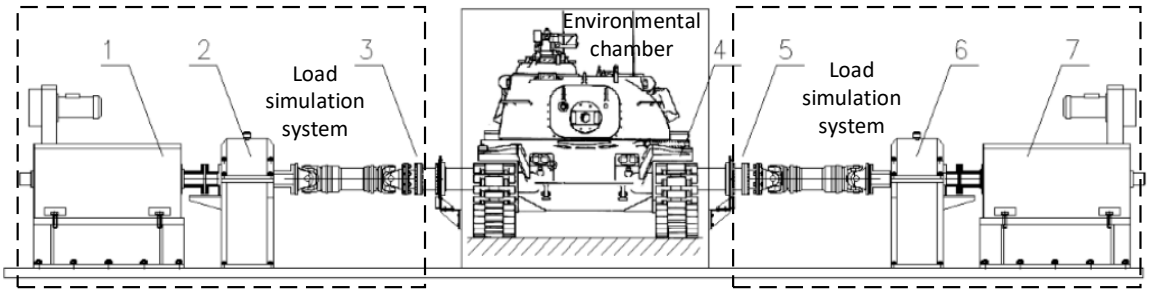


1 - electric motor, 2 - reducer, 3 - torque meter and encoder, 4 - tested vehicle, 5 - torque meter and encoder, 6 - reducer, 7 - electric motor.

**Figure 1.** Simulation test bench for tracked vehicles.

### *2.1. Dynamic Model of a Tracked Vehicle*

In order to achieve accurate load simulation, firstly, the dynamics model of the tracked vehicle needs to be analyzed to obtain the relationship between the torque and rotation speed of the driving wheel.

Tracked vehicles are subjected to the interaction of driving force, inertia force, and driving resistance in the course of driving. The force exerted on the body reaches the moment balance at the active wheel [31]. By identifying the equivalent of the force to the driving wheel, the torque formula of the driving wheel can be obtained as follows:

$$T_e + T_a + T_s + T_w + T_f = 0 \tag{1}$$

$$T_a = J_e \alpha_d \tag{2}$$

$$T_s = Rmgsin\gamma \tag{3}$$

$$T_w = \frac{RC_D A V_v^2}{21.45} \tag{4}$$

$$T = T_f + T_s \tag{5}$$

where, $\alpha_d$ is the angular acceleration of the vehicle output axle, $\gamma$ is the vehicle inclination, $C_D$ is the wind resistance coefficient, $A$ is the vehicle forward projection area, $T_e$ is the vehicle driving moment, $T_a$ is the vehicle inertia moment, $T_s$ is the slope resistance moment, $T_w$ is the wind resistance moment, $T_f$ is the ground resistance moment, T is the road resistance moment, and R is the effective radius of the driving wheel.

Because tracked vehicles often travel on complex roads, it is necessary to study their driving conditions when switching between different slopes in body dynamics modeling. In this paper, the driving conditions of tracked vehicles are divided into six processes, namely, the horizontal slope, increase of slope, downhill slope, decrease of slope, increase of slope, and decrease of slope, respectively, corresponding to stages 1 to 6 in Figure 2.

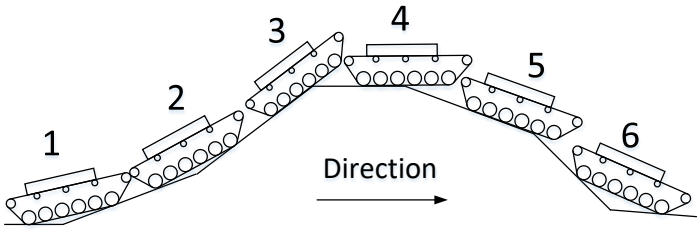


**Figure 2.** Diagram of a tracked vehicle on a slope.

Detailed slope decomposition for each stage is shown in Figure 3. In this figure, s means the up (down) slope distance, $\theta_i$(i=1,2,3,4) means the slope angle, $h_c$ means the centroid height, and $l_d$ means the relative horizontal distance between the centroid and geometric center.

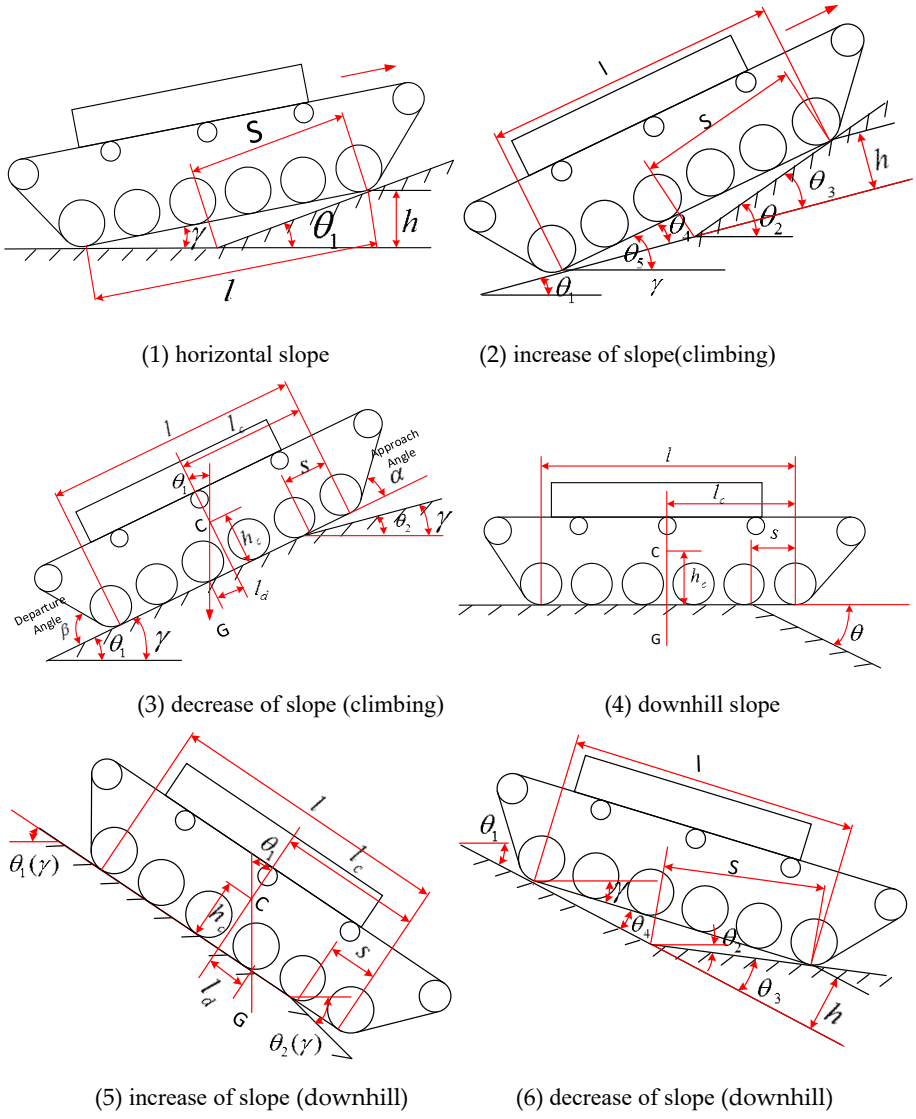


**Figure 3.** Force analysis of a tracked vehicle.

According to the above figure, the inclination angle and road resistance of the tracked vehicle at a certain instantaneous stage can be obtained. The judgment process is shown in Figure 4.

By Laplace transformation of Formula (1) to Formula (5), the vehicle dynamic equation is obtained as follows:

$$G_{em}(s) = \frac{\omega_{em}(s)}{T_e(s) - T(s) - T_w(s)} = \frac{1}{J_e s} \tag{6}$$

where $\omega_{em}(s)$ means the speed of the driving wheel and $J_e$ means the vehicle equivalent inertia.

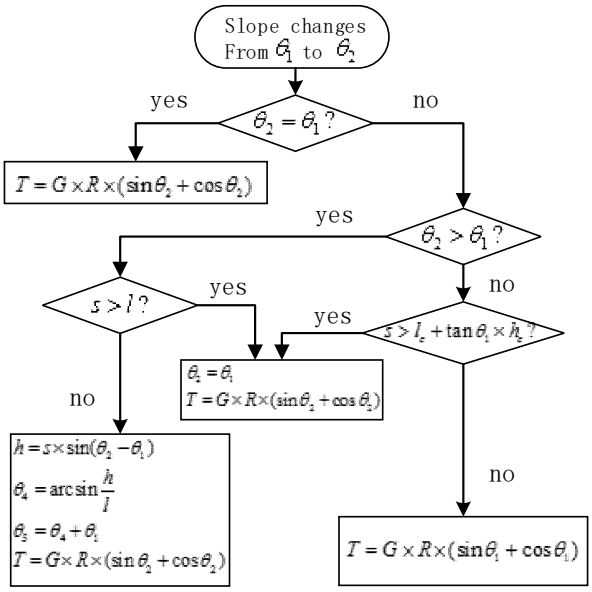


**Figure 4.** Chart of car body inclination angle and resistance moment analysis.

### 2.2. Equivalent Inertia Modeling of Tracked Vehicles

Formula (6) shows that in order to obtain $\omega_{em}(s)$, the inertia of the whole vehicle must be equivalent to the driving wheel. Equivalent analysis of the inertia of the tracked vehicle shows that

$$\frac{1}{2}(m_v v_v^2 + m_t v_t^2 + n_l J_l \omega_l^2 + J_d \omega_d^2 + J_i \omega_i^2 + n_b J_b \omega_b^2) = \frac{1}{2} J_e \omega_d^2 \tag{7}$$

where, $m_v$ means the vehicle mass (excluding track), $v_v$ means the vehicle speed, $m_t$ means the track mass, $v_t$ means the track speed, $n_l$ means the number of load wheels, $J_l$ means the load wheel rotation inertia around the axle center, $\omega_l$ means the load wheel angular speed, $J_d$ means the drive wheel rotation inertia around the axle center, $\omega_d$ means the drive wheel angular speed, $J_i$ means the induced wheel rotation around the axle center Inertia, $\omega_i$ means the angular velocity of the inducer, $n_b$ means the number of supporting roller, $J_b$ means the inertia of the supporting roller rotating around the axle center, and $\omega_b$ means the angular velocity of the supporting roller.

Equation (7) shows that the translational inertia and rotational inertia of all parts of the vehicle can be expressed by the inertia revolving around the driving wheel. In order to calculate the equivalent inertia accurately, it should be divided into three parts, as shown in Formula (8).

$$J_e = J_v + J_t + J_o \tag{8}$$

Here, $J_v$ means the vehicle body equivalent inertia (excluding the track and wheel rotational inertia); $J_t$ means the equivalent inertia of the track; and $J_o$ means other equivalent inertia, including that of the driving wheel, induced wheel, and supporting roller. These three kinds of inertia are analyzed separately below.

Figure 5 shows the relationship between body speed and driving wheel speed.

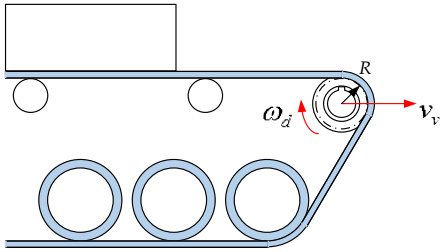


**Figure 5.** The relationship between body speed and driving wheel speed.

According to Figure 5, we can get

$$v_v = \omega_d R(1-\delta) \tag{9}$$

where $\delta$ means the slip rate between the track and ground.

So for the body, there is

$$\frac{1}{2}m_v v_v^2 = \frac{1}{2}J_v \omega_d^2 \tag{10}$$

By combining the two forms, we can get

$$J_v = m_v(R - R\delta)^2 \tag{11}$$

When $\delta = 0$, the original format becomes

$$J_v = m_v R \tag{12}$$

The biggest difference between a tracked vehicle and traditional vehicle is that a tracked vehicle is equipped with high-quality tracks [32]. Because the track is irregular and the absolute speed of each part when driving is different, it should be divided into four parts, including the upper, lower, front, and rear parts, when calculating. Assuming that the tracked vehicle is moving at a uniform speed on the ground with no relative slip, that is, the slip rate $\delta = 0$, the inertia of the grounding part of the track can be ignored. However, in a normal driving process, due to bad ground conditions (such as marsh, snow, etc.), the slip rate is usually not stable, so it is necessary to consider the total inertia of the track. To analyze it, the speed of each part is decomposed into relative speed and frame speed, which is shown in Figure 6.

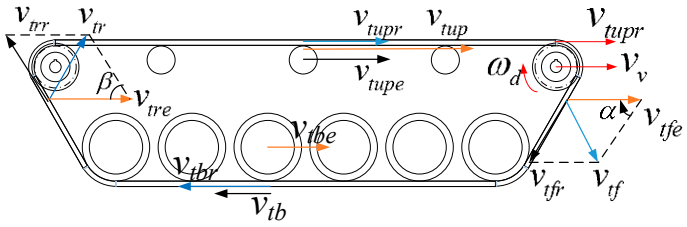


**Figure 6.** Track velocity analysis in each section.

The upper part of the track is shown in Figure 7. The absolute speed of the upper part $v_{tup}$ consists of the traction speed $v_{tupe}$ and relative speed $v_{tupr}$.

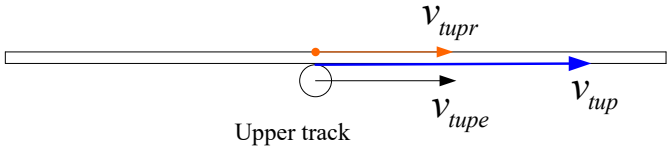


**Figure 7.** Upper part of the track.

By understanding three velocities as three vectors, we can get

$$\vec{v_{tup}} = \vec{v_{tupe}} + \vec{v_{tupr}} \tag{13}$$

According to the Vector Superposition Rule,

$${v_{tup}}^2 = {v_{tupe}}^2 + {v_{tupr}}^2 - 2v_{tupe}v_{tupr}cos\pi \tag{14}$$

where $\pi$ is the vector angle between $\vec{v_{tupe}}$ and $\vec{v_{tupr}}$.

For $v_{tupe}$, there is

$$v_{tupe} = v_v = \omega_d R(1-\delta) \tag{15}$$

Furthermore, for $v_{tupr}$, there is

$$v_{tupr} = \omega_d R \tag{16}$$

In addition, according to the law of the conservation of energy,

$$\frac{1}{2}m_{tup}v_{tup}^2 = \frac{1}{2}J_{tup}\omega_d^2 \tag{17}$$

By simultaneously considering formulae (13) to (17), we can get

$$J_{tup} = m_{tup}(2R - R\delta)^2 \tag{18}$$

For the front part of the track, the velocity relationship is shown in Figure 8. In the same way, we can derive the equivalent inertia.

$$\vec{v_{tf}} = \vec{v_{tfe}} + \vec{v_{tfr}} \tag{19}$$

$${v_{tf}}^2 = {v_{tfe}}^2 + {v_{tfr}}^2 - 2v_{tfe}v_{tfr}cos\alpha \tag{20}$$

$$v_{tfe} = v_v = \omega_d R(1-\delta) \tag{21}$$

$$v_{tfr} = \omega_d R \tag{22}$$

$$\frac{1}{2}m_{tf}v_{tf}^2 = \frac{1}{2}J_{tf}\omega_d^2 \tag{23}$$

$$J_{tf} = m_{tf}[(R - R\delta)^2 + R^2 - 2R(R - R\delta)cos\alpha] \tag{24}$$

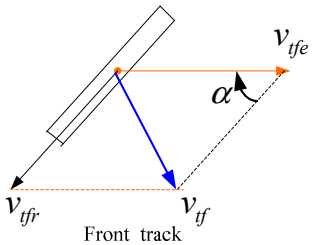


**Figure 8.** Front part of the track.

It is easy to calculate the inertia of other parts of the track by the same method.

$$J_{tb} = m_{tb}R^2\delta^2 \tag{25}$$

$$J_{tr} = m_{tr}[(R - R\delta)^2 + R^2 - 2R(R - R\delta)cos\beta] \tag{26}$$

Here, $v_{tup}$, $v_{tb}$, $v_{tf}$, and $v_{tr}$ mean the absolute speed of the upper, lower, front, and rear parts of the track; $v_{tupe}$, $v_{tbe}$, $v_{tfe}$, and $v_{tre}$ mean the traction velocity of the upper, lower, front, and rear parts of the

track; $v_{tupr}$, $v_{tbr}$, $v_{tfr}$, and $v_{trr}$ mean the relative velocity of the upper, lower, front, and rear parts of the track to driving wheel; $m_{tup}$, $m_{tb}$, $m_{tf}$, and $m_{tr}$ mean the mass of the upper, lower, front, and rear parts of the track; and $J_{tup}$, $J_{tb}$, $J_{tf}$, and $J_{tr}$ mean the equivalent inertia of the upper, lower, front, and rear parts of the track.

Therefore, the equivalent inertia of the tracked part on the driving wheel can be presented as

$$\begin{aligned} J_t = {} & m_{tup}(2R - R\delta)^2 + m_{tb}R^2\delta^2 + m_{tf}[(R - R\delta)^2 + R^2 - 2R(R - R\delta)cos\alpha] \\ & + m_{tr}[(R - R\delta)^2 + R^2 - 2R(R - R\delta)cos\beta] \end{aligned} \tag{27}$$

$J_o$ includes the inertia of the loading wheel, driving wheel, induced wheel, and supporting roller. Among them, the structure of the wheel is relatively special, because it has an I-shaped cross section, where $R_1$ is the outer diameter and $R_2$ is the inner diameter. It is shown in Figure 9.

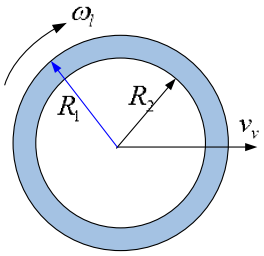


**Figure 9.** Wheel.

Using the same deduction method as above, we can get the deduction process as described in Formula (28)–(31), as follows:

$$v_v = \omega_d R(1 - \delta) = \omega_l R_1(1 - \delta) \tag{28}$$

$$J_l = \frac{1}{2}m_l({R_1}^2 - {R_2}^2) \tag{29}$$

$$\frac{1}{2}J_{lequ}{\omega_d}^2 = \frac{1}{2}n_l J_l {\omega_l}^2 \tag{30}$$

$$J_l = n_l m_l(R_1^2 + R_2^2)\frac{R^2}{R_1^2} \tag{31}$$

In the same way, we can get the equivalent inertia of other rollers:

$$J_i = m_i R^2 \tag{32}$$

$$J_b = n_b m_b R^2 \tag{33}$$

The equivalent inertia of the whole vehicle in the driving wheel can be obtained by synthesizing the formula above, that is,

$$\begin{aligned} J_e = {} & m_{tup}(2R - R\delta)^2 + m_{tb}R^2\delta^2 + m_{tf}[(R - R\delta)^2 + R^2 - 2R(R - R\delta)cos\alpha] \\ & + m_{tr}[(R - R\delta)^2 + R^2 - 2R(R - R\delta)cos\beta] + n_l m_l(R_1^2 + R_2^2)\tfrac{R^2}{R_1^2} + m_i R^2 \\ & + n_b m_b R^2 + m_v R^2(1 - \delta)^2 \end{aligned} \tag{34}$$

According to the output torque of the vehicle and the equivalent inertia of the tested vehicle, the target speed of the vehicle can be deduced.

## 3. Control Strategy

When testing the power system of a vehicle on the bench, it is the primary task of the bench to exert a load equal to the actual working condition. For the test bench in this paper, the task of the control system is to accurately simulate the driving resistance of the tracked vehicle [33].

In order to achieve this function, the driving moment $T_e$ of the tested vehicle is measured by the torque sensor, and the theoretical rotational speed $\omega_{em}$ of the driving wheel can be obtained by substituting $T_e$ into Formula (6). When the combined torque of $T_e$ and output torque of the load analog motor makes the system rotate, the current rotational speed $\omega$ is obtained by the sensors and a controller C is designed to make $\omega$ infinitely approach $\omega_{em}$, so that the simulation of vehicle driving resistance can be realized. The system control block diagram is shown in Figure 10, where G(s) and J(s) are the transfer function of the motor and transmission mechanism, respectively.

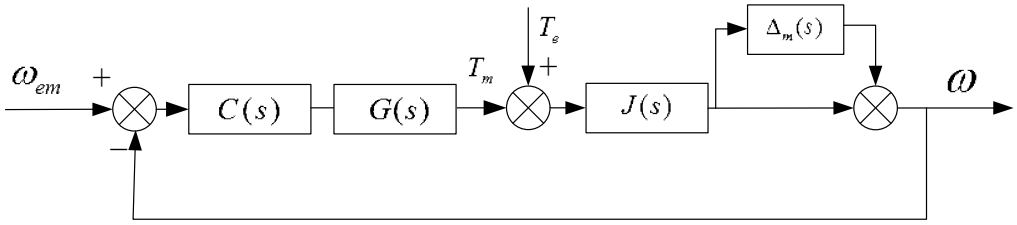


**Figure 10.** Control block diagram of the load simulation system.

As can be seen from the above figure, the control method is actually used to track the speed response of the system under the current torque. However, in the actual operation process, because the system is affected by environmental factors and friction coefficients at different velocities, a non-linear uncertainty $\Delta(s)$ exists in its transfer function. In addition, the system loop is also affected by the driving torque $T_e$, which is an external additional torque for the whole load simulation system. [34,35]. However, in practice, the system is driven by the combined torque of $T_e$ and $T_e$. For the control loop, $T_e$ is not controlled by the system and is controlled by the external controller on the test vehicle or throttle. Therefore, for the load simulation system, $T_e$ is an uncontrollable random variable, and when it changes dramatically, it is very likely that the system will deviate from the target speed. Because of this, when $\Delta(s)$ changes or $T_e$ mutations occur, the stability of the system is problematic. In this regard, it is necessary to design a controller C which can not only adjust the loading and transmission system, but also respond quickly and follow $\omega_{em}$ under the action of system disturbance torque.

There is an intuitive idea that the robust control method can be used to design the controller C(s) by taking the maximum disturbance and the maximum uncertainty of the test-bed system as the disturbance rejection index of the system and combining it with the tracking requirement of $\omega_{em}$ [36,37]. However, for a single controller, the responsiveness and strong anti-jamming ability are contradictory. Therefore, according to the structural invariance principle, the system is designed as a 2-degree-of-freedom loop (2-DOF), as shown in Figure 11. In the figure, $\xi$ is the sensor noise, $G_n(s)$ is the nominal transfer function of the system, $G_n(s) = G(s) \cdot J(s)$, and Q(s) is the filter to be designed. The disturbance observer (DOB) composed of Q(s) and ${G_n}^{-1}(s)$ in the dashed line frame is used to suppress the disturbance of the system, enhance the robustness of the system, and make the system transfer function close to the nominal transfer function $G_n(s)$. The DOB and the controlled system constitute the inner loop of the system [38]. The outer loop is controlled by controller C. Since the disturbance observer in the inner loop has suppressed the disturbance and noise of the system, the outer loop controller only needs to control the response speed and steady-state error of the system. According to the design requirements and test experience, controller C needs to control the response time of the system within 100ms and the tracking error within 1%.

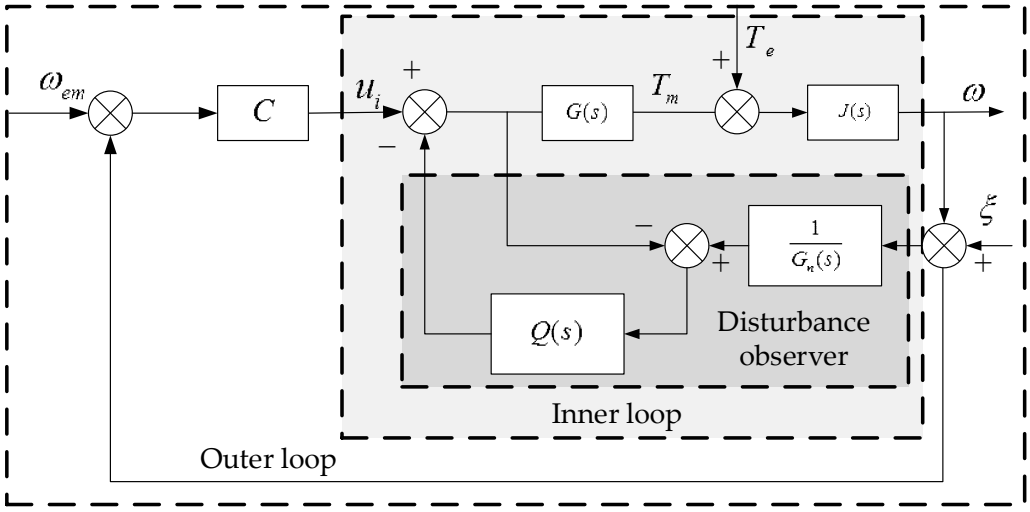


**Figure 11.** Control loop with a disturbance observer.

For the disturbance observer in the inner loop, because $G_n(s)$ is usually regular, ${G_n}^{-1}(s)$ is irregular and not realizable, so it is necessary to introduce a filter Q(s) to make Q(s)${G_n}^{-1}(s)$ realizable. Therefore, it is required that the relative order of Q(s) be greater than or equal to that of $G_n(s)$, that is, $k_Q \geq k_G$. The closed-loop transfer function of the inner loop can be obtained when the effects of $T_e$ and $\Delta$(s) on the system are collectively referred to as disturbances and defined as d.

$$y = G^y_{u_i}(s)u_i + G^y_d(s)d + G^y_\zeta(s)\zeta \tag{35}$$

where

$$G^y_{u_i}(s) = \frac{y}{u_i} = G_n(s) \tag{36}$$

$$G^y_{d_1}(s) = \frac{y}{d} = G_n(s)(1 - Q(s)) \tag{37}$$

$$G^y_\zeta(s) = \frac{y}{\zeta} = Q(s) \tag{38}$$

It can be seen that the effect of disturbance and noise on the system results is determined by Q(s) and 1-Q(s). Here, Q(s) is the sensitivity function of the system and 1-Q(s) is the complementary sensitivity function of the system. For the systems, since disturbances usually occur in the low-frequency band and noise usually occurs in the high-frequency band, it is necessary to design a low-pass filter Q(s) to suppress ξ in the high-frequency band and 1-Q(s) to suppress d in the low-frequency band.

Using the above control method, a set of load simulation equipment consisting of a direct current motor (DC) and mechanical transmission equipment is simulated in this paper. The transfer function of the DC motor is known as

$$G(s) = \frac{T_m(s)}{u_i(s)} = \frac{4798}{0.000743s^2 + 0.00726s + 1} \tag{39}$$

The transfer function of the mechanical transmission equipment is

$$J(s) = \frac{\omega(s)}{T_m(s)} = \frac{1}{507s + 24} \tag{40}$$

By simultaneously considering the two formulas, we can get

$$G_n(s) = \frac{T_m(s)}{u_i(s)} \cdot \frac{\omega(s)}{T_m(s)} = \frac{4798}{(0.000743s^2 + 0.00726s + 1)(507s + 24)} \tag{41}$$

Based on the above conditions, the DOB for the system with the transfer function $G_n(s)$ is designed by using the $H_\infty$ mixed sensitivity method. The optimal filter transfer function is

$$Q(s) = \frac{1.86 \times 10^{12}}{(s + 1.484)(s^2 + 5.4 \times 10^4 s + 1.26 \times 10^{12})} \tag{42}$$

The outer loop controller $C(s)$ is designed as the PI controller, and the transfer function is

$$C(s) = \frac{0.4s + 1.48}{s} \tag{43}$$

According to the above model, a tracked vehicle with an equivalent inertia of 3180 kg·m$^2$ is simulated. The control model is established in Simulink and the speed response under a random torque signal is simulated, and the results are shown in Figure 12. Because of the large amplitude transformation of random signals, this type of signal also acts as the interference signal affecting the system, and the output speed deviates greatly from the theoretical speed under the control of the traditional 1DOF loop. Furthermore, by applying the 2DOF system with DOB described in this paper, it is found that the speed deviation of the system decreases significantly. Therefore, it can be seen that the control loop has an obvious effect on stabilizing the system and reducing the deviation.

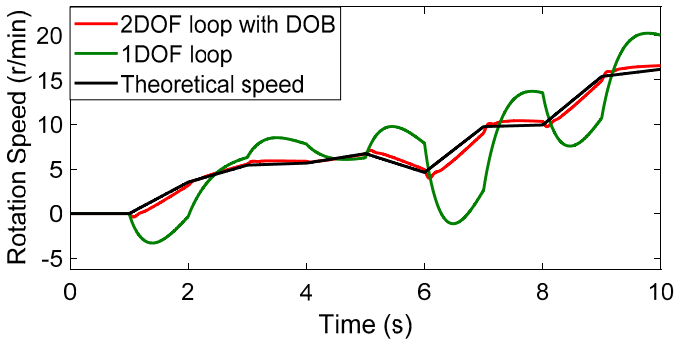


**Figure 12.** Speed response under different control modes.

## 4. Calibration of Electrical Inertia Simulation Accuracy

In order to study the accuracy of the electrical inertia simulation, the driving shaft and gearbox were used to connect the two ends of the tested motor to remove the intermediate vehicle, as shown in Figure 13. At this time, the right analog end simulates the inertia load by using the speed tracking method, and the left driving motor imposes a preset load. According to Formula (44), when the system torque is known, instantaneous acceleration of the system can be obtained by deriving the system speed, and the inertia of the instantaneous motor simulation can be obtained. Comparing the measured inertia with the standard inertia, the electric inertia can be calibrated.

$$T_i = J\alpha \tag{44}$$

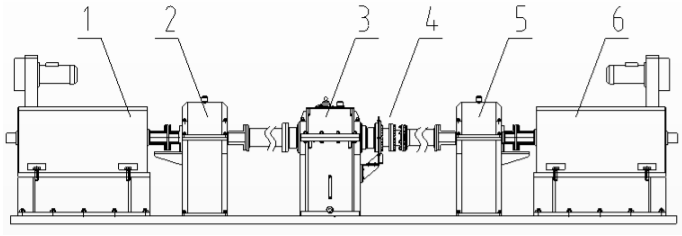


1 - electric motor, 2-reducer, 3-reducer, 4 - torque sensor, 5 - reducer, and 6 - tested motor

**Figure 13.** Structure of the electric inertia calibration test bench.

### *4.1. Calibration of Standard Inertia*

In the electrical inertia simulation test, the main factors affecting the accuracy of the test results are the accuracy of the inertia simulation and the system response time [39]. In this paper, a set of calibrated high-precision standard inertia boxes are used to calibrate the electric inertia.

Suppose that the inertia of one stage in the flywheel box and driving components to be calibrated is $J_s$ and $J_{ba}$, respectively. Then, the inertia to be simulated by the motor is $J_a$. To achieve $J_{ba} \pm J_a = J_s$, the inertia box and the tested motor are driven with the same torque to obtain the speed-up curve. By comparing the experimental results of the two groups, the calibration of the electric inertia simulation is completed.

The mechanical structure of the standard inertia (flywheel box) test is shown in Figure 14. According to Formula (44), when the input torque is constant, the speed of the system should rise uniformly in a constant angular acceleration $\alpha$. Therefore, the standard inertia of the system can be calculated by the input torque and the measured velocity curve. In practical experiments, the formula is modified to $T_t - T_d = J\alpha$ because of the resistance of the system, which is mainly related to the rotation speed [25,28]. When the rotation speed of the system is at a proper level, the resistance of the system is basically stable. Therefore, the angular acceleration can be measured by changing different driving torques, and the standard inertia of the system can be obtained by two sets of equations.

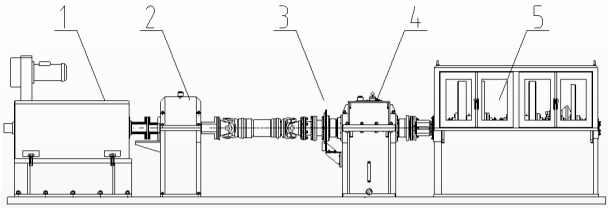


1 - electric motor, 2 - reducer 3 - torque meter, 4 – reducer, 5 - standard inertia flywheel box

**Figure 14.** Structure of a standard inertia calibration test.

As shown in Figure 15, the driving torque values $T_{t1}$ and $T_{t2}$ are set separately at different stages of the same test, and the acceleration values $\alpha_1$ and $\alpha_2$ corresponding to the stage of higher speed curve steady speed rise $(r_1 \sim r_2)rpm$ are selected. Because the acceleration at the same speed is collected at different stages, it is considered that the resistance $T_{di}$ of each stage is equal. The inertia value $J_s$ of the standard inertia disc can be calculated by taking the difference between $T_{t1}$ and $T_{t2}$. The accuracy of the standard inertia simulation is thus verified.

$$T_{t1} - T_{d1} = J_s\alpha_1 \tag{45}$$

$$T_{t2} - T_{d2} = J_s\alpha_2 \tag{46}$$

$$J_s \approx \frac{T_{t1} - T_{t2}}{\alpha_1 - \alpha_2} \tag{47}$$

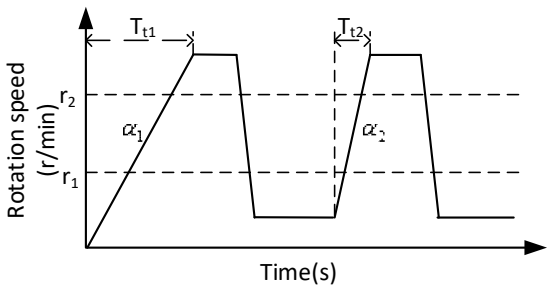


**Figure 15.** Test flow.

The actual structure of the standard inertia box is a flywheel set with large inertia, and its inertia simulation range is (50–1000) kg·m$^2$. In order to improve the upper limit of inertia simulation and provide more reference data for electric inertia simulation calibration, a gearbox equipped with speed ratios of 1:2.36 and 1:6.48 is equipped to improve the equivalent inertia of the equipment being marked. The maximum equivalent inertia of the original 1000 kg·m$^2$ is 42,006.60 kg·m$^2$ after considering the gear box deceleration ratio. That is to say, the inertia ranging from 255–42,000 kg·m$^2$ can be simulated by different combinations of inertia plates in the flywheel box. In this simulation method, although it is a simulation, through data processing, it can completely reflect the data curve within 250~41,000, to meet the requirements of comparison. In this way, the inertia calibration test of 400 kg·m$^2$ inertia box with a 1:2.36 transmission ratio is carried out. The test results are shown in Figure 16.

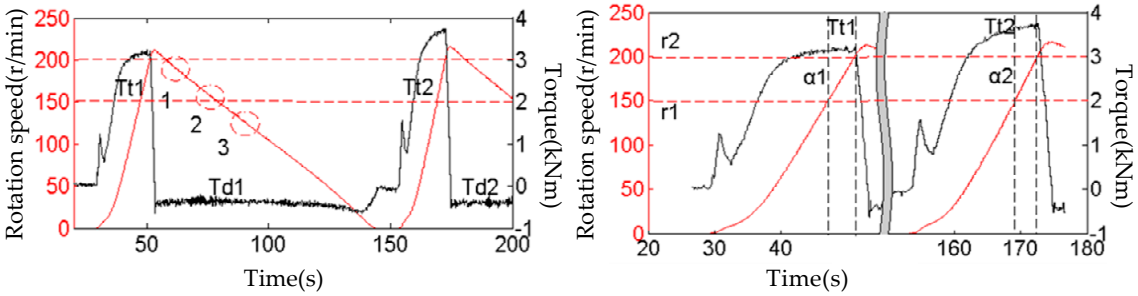


(a) Overall data (b) Data of calibration

**Figure 16.** Calibration test results under equivalent inertia of 2227.84 kg·m$^2$.

Figure 16a is the overall data of the test while Figure 16b is the calibration section. In the test, the equivalent inertia of the flywheel is 2227.84 kg·m$^2$. The average acceleration of the system is 1.3 rad/s$^2$ under the condition of average torque $T_{t1}$ = 3140.09Nm, and 1.54 rad/s$^2$ under the condition of $T_{t2}$ = 3674.7 Nm. Therefore, the inertia of the system is 2229.94 kg·m$^2$ and the measurement deviation is 0.19%.

Observing the two deceleration processes, it can be found that the speed decline curve of the system during the deceleration process is smooth, and there is no obvious fluctuation in the $T_{d1}$ and $T_{d2}$ of the torque curve section. The deceleration of the system is 0.24, 0.23, and 0.23 rad/s$^2$, respectively, when analyzing the deceleration of the system at the intervals of 1, 2, and 3. Therefore, the influence of system resistance moment on the inertia calibration of the test-bed in a high speed range can be neglected.

The standard inertia of 750 kg·m$^2$ can be calibrated in the same way at the transmission ratio of 1:2.36, shown in Figure 17. The equivalent inertia is 4177.2 kg·m$^2$. Under the condition of average torque $T_{t1}$ = 4220.38 Nm, the average acceleration of the system is 0.94 rad/s$^2$, while under the condition of $T_{t2}$ = 4919.48 Nm, the average acceleration of the system is 1.11 rad/s$^2$. Therefore, the inertia of the system is 4157.79 kg·m$^2$ and the measurement deviation is 0.46%.

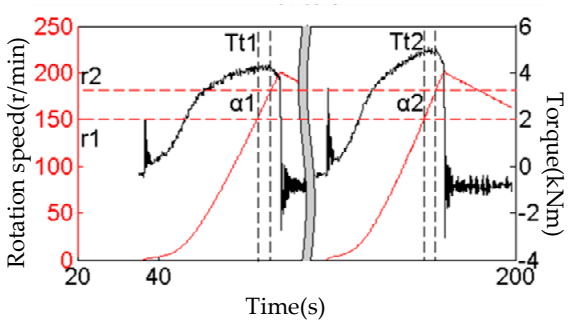


**Figure 17.** Calibration test results under equivalent inertia of 4177.2 kg·m$^2$.

The standard inertia of 250 kg·m$^2$ can be calibrated at the transmission ratio of 1:6.48, shown in Figure 18. The equivalent inertia is 10,497.6 kg·m$^2$. Under the condition of average torque $T_{t1} = 7206.53$ Nm, the average acceleration of the system is 0.67 rad/s$^2$, while under the condition of $T_{t2} = 4919.48$ Nm, the average acceleration of the system is 0.73 rad/s$^2$. The inertia of the system is 10,522.34 kg·m$^2$ and the measurement error is 0.23%.

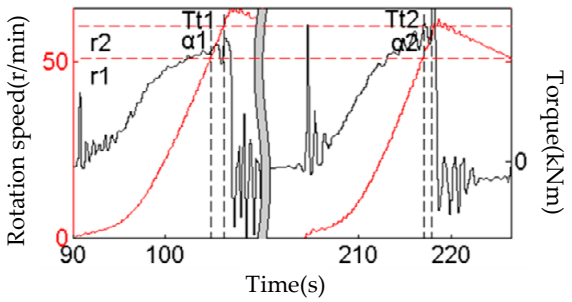


**Figure 18.** Calibration test results under equivalent inertia of 10497.6 kg·m$^2$.

The variation of standard inertia deviation with the increase of equivalent inertia is shown in Figure 19. It is evident that the mechanical inertia under large inertia is less than 0.5%, except in the case of small inertia, where the inertia calibration deviation is too large due to fluctuation of the sensor signal.

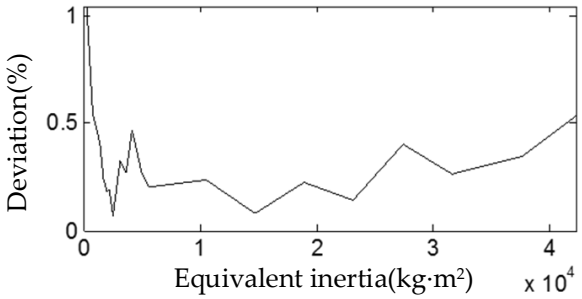


**Figure 19.** Deviation of standard inertia.

### *4.2. Calibration of Basic Inertia*

Through the standard inertia test, the inertia $J = J_s$ of each test system can be determined. Because the inertia simulation equipment itself has inertia $J_{ba}$ (which is called the basic inertia of the system for convenience of expression), it is necessary to define the basic inertia $J_{ba}$ of the equipment before the electrical inertia simulation test, so that the simulation inertia $J_\alpha$ of the motor can be defined.

$$J_s = J_{ba} + J_\alpha \tag{48}$$

To calibrate the basic inertia, mechanical connection is adopted, as shown in Figure 20. The to-be-calibrated inertia includes the tested motor (6), reducer (5), torque meter (4), and coupling. During the test, the driving end is in torque control mode, and the calibrated end is powered off. Under this structure, the basic inertia $J_{ba}$ of the system can be obtained by the same principle as the standard inertia.

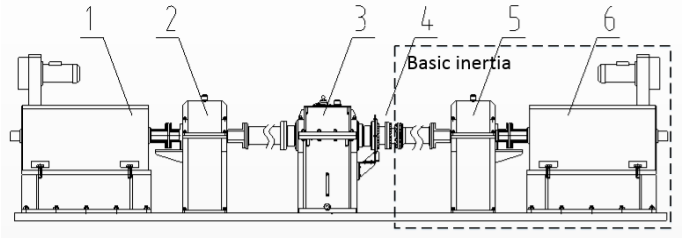


1 electric motor, 2-reducer, 3-reducer, 4 - torque sensor, 5 – reducer, and 6 - tested motor.

**Figure 20.** Structure of a basic inertia calibration test.

The test result is shown in Figure 21. According to the design and manufacture drawings, the theoretical basic inertia is 512 kg·m$^2$. The average acceleration of the system is 1.79 rad/s$^2$ during the speed 150~200 r/min under the condition of average torque $T_{t1}$ = 1500Nm, and 2.02 rad/s$^2$ under the torque of $T_{t2}$ = 1620 Nm. The actual inertia is 523.96 kg·m$^2$ after calibration.

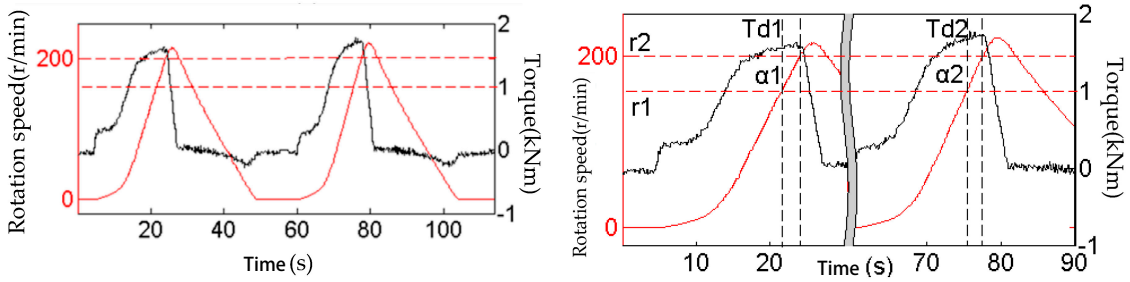


(1) Overall data (2) Data of calibration section

**Figure 21.** Test results of basic inertia calibration.

### *4.3. Calibration of Electrical Inertia*

In the standard inertia calibration test, the test result of 400 kg·m$^2$ inertia flywheel set at a 1:2.36 transmission ratio is 2232.05 kg·m$^2$. As the basic inertia is known to be 523.96 kg·m$^2$, the inertia to be simulated by the electric motor is 1708.09 kg·m$^2$. After calibrating in the same way as the standard inertia calibration, the experimental results are shown in Figure 22. The system inertia is 2211.09 kg·m$^2$ and the percentage deviation of the electrical inertia simulation is 0.95%.

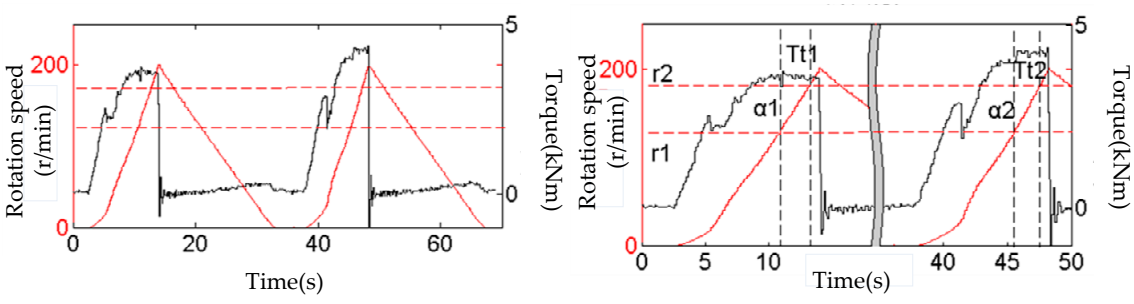


(1) Overall data (2) Data of calibration section

**Figure 22.** Test results under equivalent inertia of 2232.05 kg·m$^2$.

With the same method, the equivalent inertia of 750 kg·m$^2$ and 250 kg·m$^2$ in the standard inertia calibration test is 4157.69 kg·m$^2$ and 10,522.34 kg·m$^2$ respectively. Through the calibration shown below, the inertia and percentage deviation of the two groups are 4183.43 kg·m$^2$ (0.61%) and 10,603.38 kg·m$^2$ (0.76%), respectively, shown in Figure 23.

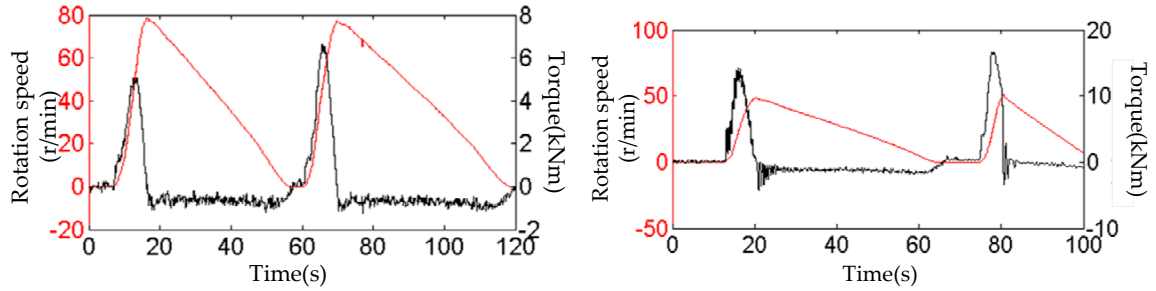


(1) Inertia of 4157.69kgm$^2$ (2) Inertia of 10522.34kgm$^2$

**Figure 23.** Calibration test results under equivalent inertia of 4157.69 kg·m$^2$ and 10,522.34 kg·m$^2$.

The variation of electrical inertia simulation deviation with the increase of equivalent inertia is shown in Figure 24. It can be found that in the range of inertia of 1000~30,000 kg·m$^2$, the deviation is less than 1%. The trend of simulation deviation of electrical inertia is the same as that of standard inertia.

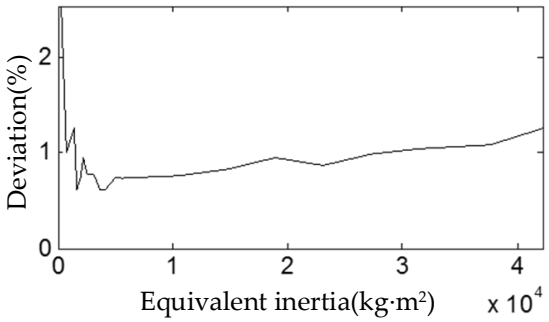


**Figure 24.** Simulated deviation of electrical inertia.

### *4.4. Calibration of Electrical Inertia Response Time*

When the motor is used to simulate mechanical inertia, there must be a delay problem, so the response time of the system needs to be measured [40,41]. According to $T_t - T_d = J\alpha$, it can be seen that when the driving torque $T_t$ of the system is set as a constant value and the resistance moment $T_d$ of the system is basically stable, the angular acceleration $\alpha$ is a constant value. The corresponding angular acceleration curve can be obtained by measuring the rotational speed of the system. When the angular acceleration of the system is stable, the electrical inertia simulated by the system is stable. Therefore, the response time of the electrical inertia simulation of the measurement system can be obtained by observing the angular acceleration (or torque) curve.

As shown in Figure 25, the electric inertia is calibrated by the steady acceleration test. Under the stable torque condition, the system uses the motor to follow the target speed through the step acceleration test. In the dotted line amplification area of Figure 25a (i.e., Figure 25b), the target velocity jumps from step to 10 r/min at 20.950 s, and then the acceleration of the system starts to respond at 20.952 s, and returns to stability at 21.022 s. By evaluating the acceleration response, the system response time of electrical inertia simulation is 72 ms.

The above calibration method can be used to calibrate the response time of electric inertia under steady state conditions. However, in the process of driving load simulation, the speed and torque of the system are often unsteady, so the above calibration results cannot express the response rate of electric inertia in a real vehicle simulation environment.

According to the speed tracking method, the system deduces the target speed $\omega_{em}(s)$ of the system through the actual system model $G_{em}(s)$, and then calculates the required motor torque $T_l(s)$ by the speed closed loop. According to a series of standard inertia tests, the change of $T_d$ in a continuous speed range can be neglected. When the output of load torque is accurate, the response time of the system can be evaluated by comparing the target acceleration $\alpha_t$ with the measured acceleration $\alpha_r$.

At the moment $t_0$ of a continuous torque fluctuation curve, the target acceleration of the system is $\alpha_t$, assuming that after t seconds $\left|\frac{\alpha_r-\alpha_t}{\alpha_r}\right| < 1\%$, the response time of the signal is considered to be $t$.

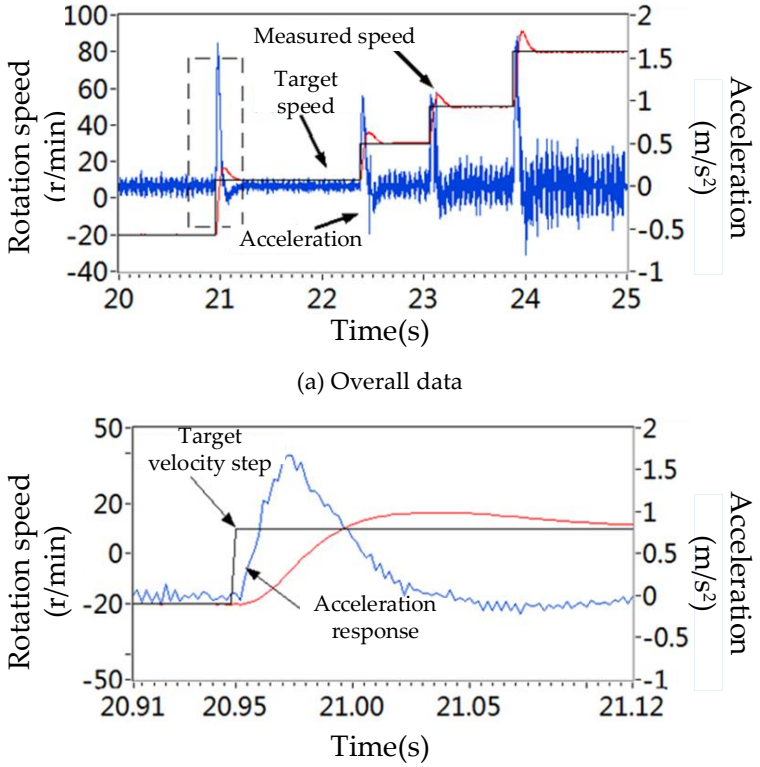


(a) Overall data




(b) Amplification area

**Figure 25.** Electrical inertia response time at constant torque.

In the actual operation process, because the sampling rate of the system is much higher than the response time of the system, the single response time adopts the following logical judgment method, in which $\Delta t$ is the sampling frequency of the system. After counting m times, the average response time of the system is $\frac{1}{m}\sum_{i=1}^{m} t_i$, as shown in Figure 26.

As can be seen in Figure 27, the response time is represented by a gray histogram. According to the logical judgment of a single response time, the average response time of the system is 25.40 ms in a preset spectrum test with continuous load variation. The slowest response of system torque occurs in several periods when the torque fluctuates greatly. At this time, the system speed fluctuates repeatedly. Because of the system lag, it is difficult for the system to respond in time, and the maximum response time is 68 ms.

Using the above methods, the response time of the control system can be calibrated in the simulation process. At present, in order to speed up the response of the system, lag compensation (such as Smith prediction), auto-disturbance rejection (ADRC), and several intelligence algorithms (such as the model reference adaptive algorithm) are generally used in the control system. The real system response speed after using this control method can be calibrated by the method described in this paper.

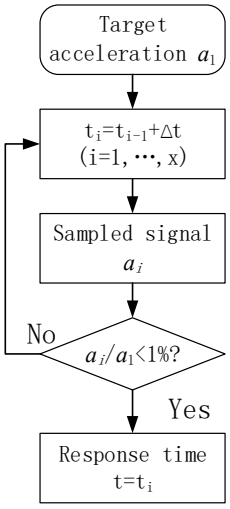


**Figure 26.** Logical judgment of a single response time.

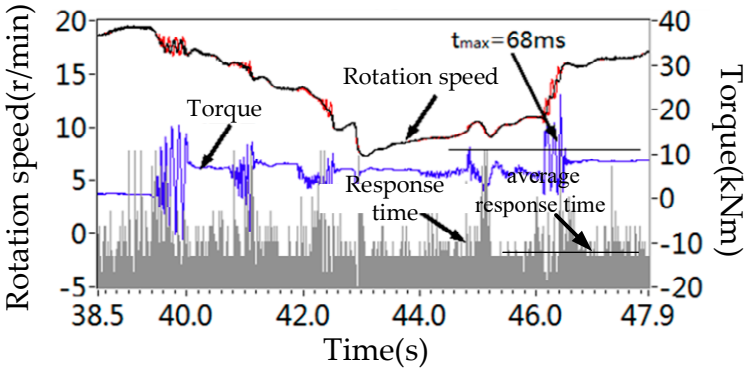


**Figure 27.** The system response time under the preset path spectrum.

## 5. Vehicle Tests

### *5.1. Correction of the Test Bed*

Before the test, the calibration results should be used to correct the system. It is known that there is a tracked vehicle with a mass of 30 t. The equivalent inertia J = 2723.6 kg·m$^2$ is obtained from Formula (34), and the input inertia of the system corrected from Figure 24 should be 2703.05 kg·m$^2$. The system is simulated with the inertia before and after correction as the input, and the experimental curve shown in Figure 28 is obtained. The results are shown in Table 1.

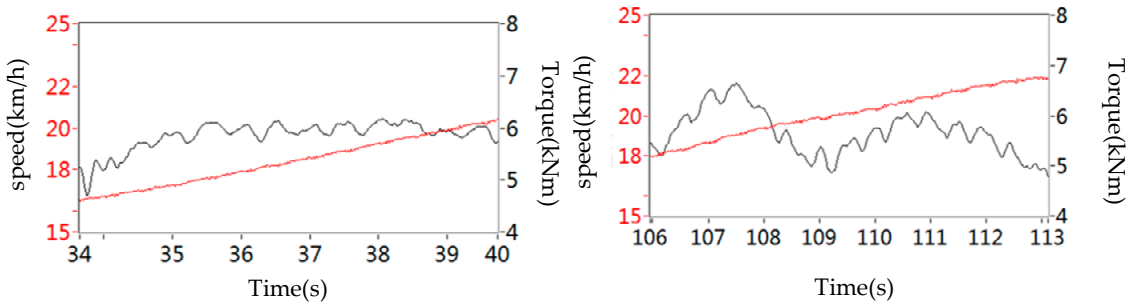


**Figure 28.** Comparison of results before and after correction.

**Table 1.** Comparison of results before and after correction.

| | Before | After |
|---|---|---|
| Input inertia/kg·m$^2$ | 2703.05 | 2723.6 |
| Angular acceleration/rad·s$^{-2}$ | 0.61 | 0.538 |
| Theoretical torque/Nm | 5861.01 | 5669.29 |
| Measured torque/Nm | 5804.51 | 5654.23 |
| Deviation | 0.96% | 0.27% |

The results show that under the same simulated object, the corrected input inertia reduces the simulation error from 0.96% to 0.27%, and effectively improves the accuracy of electrical inertia simulation.

### *5.2. Load Test and Shift Performance Test*

A load test is used to simulate the torque output of a vehicle under a specific road resistance coefficient. The accuracy of vehicle inertia modeling can be verified by a load test. Load tests were carried out on a tracked vehicle with a mass of 30 t. According to Formula (34), the equivalent inertia is J = 2723.6 and the road resistance coefficient is set to 0.05, so the road resistance moment is −4204 Nm.

Figure 29a shows the gearshift process of the tracked vehicle on a flat road. Figure 29b is a local amplification of uniform acceleration in a fixed gear. Its acceleration is 0.65 km/h, i.e., a = 0.63 rad/s$^2$. The required torque under the above equivalent inertia and deceleration is as follows:

$$T = J\alpha = 2723.6 \times 0.63 = 1724.03 \text{ Nm}$$

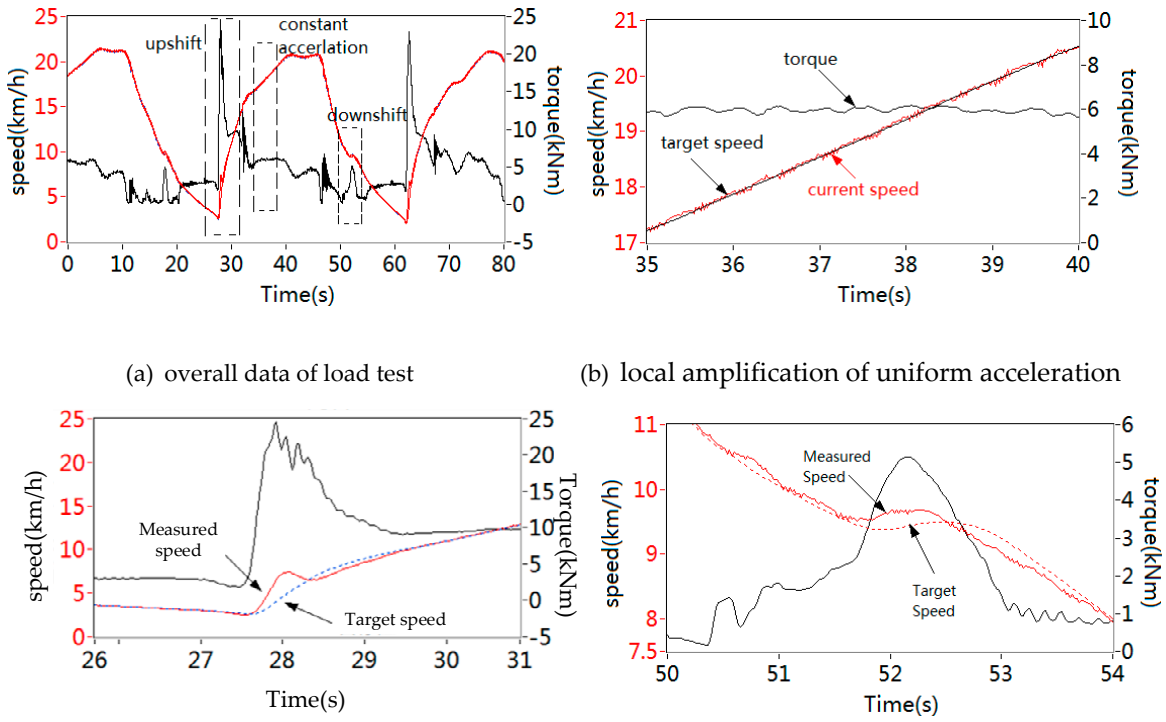


(a) overall data of load test

(b) local amplification of uniform acceleration

(c) upshift

(d) downshift

**Figure 29.** Load and shift test.

Therefore, the required torque in the above period should be

$$T = 4204 + 1724.03 = 5928.03 \text{ Nm}$$

While the actual average value is 5957.2 Nm and the relative error is 0.49%.

Figure 29c is a local zoom-in of the upshifting. In a normal shifting process, the power is released before shifting, so the system has instantaneous deceleration; after a high gear, due to the increase of the clutch front-end speed, explained by the clutch disc engagement process due to the speed difference between the front and rear discs, instantaneous large torque mutation occurs. Figure 29d is the local enlargement of downshifting. When the clutch is released after shifting, the speed of the front end of the clutch is greater than that of the back end, so the output torque has a sudden change process. In the process of the rapid change of torque, the difference between the actual speed and the target speed becomes larger due to the lag of loading of the control system. However, after the shift is completed, the speed error converges rapidly, and there is no big fluctuation in the shift process of the speed tracking control bench test. The maximum speed error is controlled within 2 km/h. The load simulation test results show that the accuracy of the equipment simulation vehicle engine load is controlled within 1%, and thus has a high accuracy.

### *5.3. Longitudinal Slope Passability Test*

A longitudinal slope passability test is used to measure and study the passability of different gradients. Through the test, the load of vehicle transmission equipment on different gradient pavement and whether the vehicle skids due to insufficient adhesion can be studied.

The same tracked vehicle as that from the load test is used. The resistance coefficient of the road surface is set to be f = 0.05. As shown in Figure 30, the designed vehicle passes through the climbing section with the gradient of 4 to 20 degrees and the downhill section with the gradient of 20 to 2 degrees. By enlarging the enlarged area of the 10 to 5 degrees section in the figure, it can be found that the vehicle will enter an adjustment area where the speed rises to slow down and the torque falls to increase when the slope changes. This phenomenon accords with the actual situation of vehicles. When the deviation between the actual speed and the target speed increases in the adjustment area, because the car body is in a dynamic change process at this time, the car body inclination angle is constantly changing. At this time, the system load suddenly falls back and the drop rate increases, which causes the system loading lag to cause the error to increase. The simulated working conditions of vehicles in five simulated area have been evaluated. At this time, the average resistance torque of the road slope is 11,528 Nm. At this time, the average load of vehicles is 11,573 Nm, and the simulation error of equipment is 0.39%, which verifies the accuracy of the dynamic model.

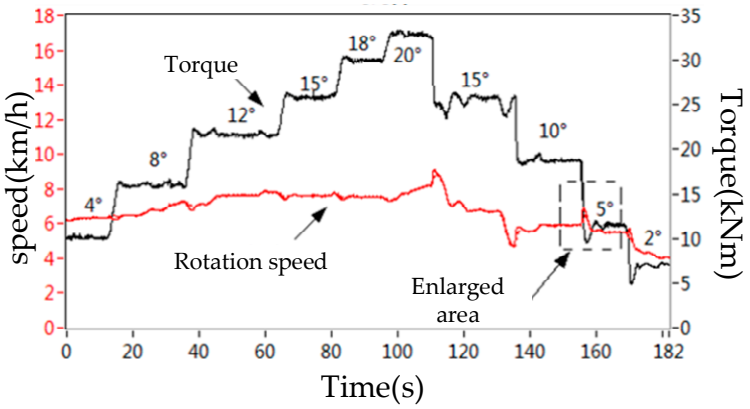


(1) Overall test data

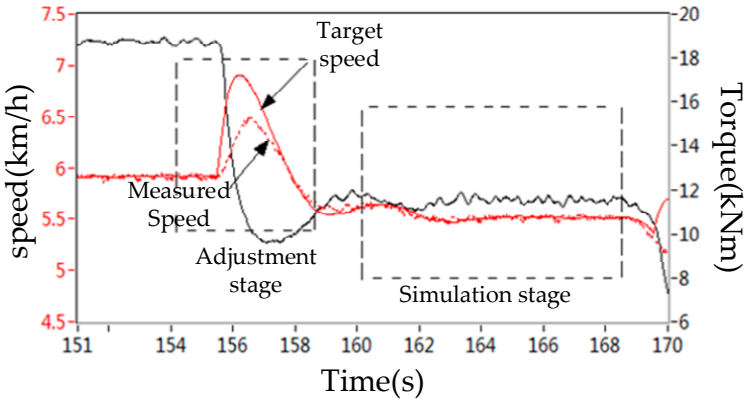


(2) Test data in enlaged area

**Figure 30.** Longitudinal slope passing test.

### 5.4. Acceleration Test

For general tracked vehicles, the acceleration capability of 0–32 km/h indicates their acceleration characteristics. In this study, in order to study the acceleration capability of tracked vehicles at different speed stages, six experiments at different speeds were carried out respectively. The maximum steady speed of tracked vehicles was evenly distributed from 9.8 km/h to 58.85 km/h. Figure 31 is the speed and torque diagram and Table 2 presents the data.

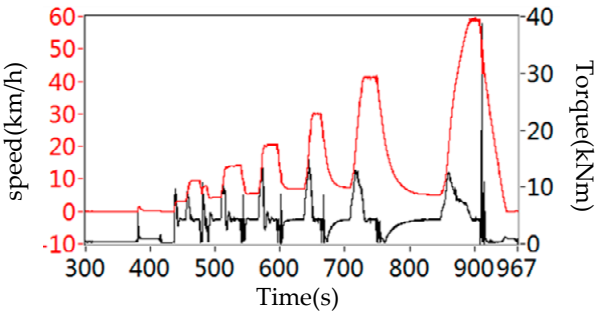


**Figure 31.** Acceleration test.

**Table 2.** Acceleration test.

| Number | Minimum Speed (km/h) | Maximum Speed (km/h) | Acceleration Time (s) | Average Acceleration ($m/s^2$) |
|---|---|---|---|---|
| 1 | 3.32 | 9.08 | 5.15 | 0.31 |
| 2 | 4.65 | 13.52 | 5.93 | 0.41 |
| 3 | 5.85 | 20.21 | 6.84 | 0.58 |
| 4 | 7.10 | 28.92 | 9.00 | 0.67 |
| 5 | 7.84 | 40.99 | 15.26 | 0.61 |
| 6 | 5.46 | 58.85 | 34.85 | 0.43 |

According to the experimental results, the tracked vehicle has the greatest acceleration capacity in the 5–40 km/h stage. When the speed exceeds 40 km/h, the acceleration capacity of the vehicle decreases due to the increase of the gear. The experimental results are in accordance with the actual vehicle acceleration performance.

## 6. Conclusions

According to the test requirement of a tracked vehicle, this paper has formulated a method that can be employed to build the equivalent inertia model of a tracked vehicle. Based on the model, a 2DOF control loop combined with a disturbance observer is proposed, which solves the stable problem due to the uncertainty and disturbance in the model. In order to discuss the accuracy of inertia simulation under the control program, this paper innovatively proposes a calibration method of inertia simulation. The test results can be used to draw the following conclusions:

(1) The 2DOF control loop combined with a disturbance observer has a good accuracy and fast response speed;

(2) The disturbance observer can effectively solve the system stability problem under model uncertainty and system disturbance;

(3) The calibration method of electrical inertia simulation using a standard inertia ratio has a good feasibility, quantitative analysis of the accuracy of mechanical inertia point simulation, and a high reference value for evaluating the control system and mechanical system;

(4) The inertia simulation accuracy of the calibrated inertia simulation system of tracked vehicles is accurate and reliable, which provides a reliable test basis for the design and development of tracked vehicles.

**Author Contributions:** Conceptualization, methodology, validation, formal analysis, investigation, writing—original draft preparation, writing—review and editing, visualization, project administration: H.L. Supervision, funding acquisition: X.Z. Resources: C.Y. Software: Z.W. Data curation: Y.F.

**Funding:** This research received no external funding.

**Acknowledgments:** This work was supported by a grant from Hangzhou BYMOON Technology Co., Ltd. The authors would like to thank Zhou for excellent technical support and Yang for critically reviewing the manuscript.

**Conflicts of Interest:** The authors declare no conflict of interest.

## Nomenclature

| | |
|---|---|
| $A$ | Vehicle forward projection area |
| $C_D$ | Wind resistance coefficient |
| $d$ | Perturbation of system |
| $h_c$ | Centroid height |
| $J_a$ | Inertia to be simulated by motor |
| $J_b$ | Inertia of supporting roller rotating around axle center |
| $J_{ba}$ | Basic inertia |
| $J_l$ | Load wheel rotation inertia around axle center |
| $J_d$ | Driving wheel rotation inertia around axle center |
| $J_i$ | Induced wheel rotation around axle center Inertia |
| $J_e$ | Vehicle equivalent inertia |
| $J_v$ | Vehicle body equivalent inertia |
| $J_t$ | Track equivalent inertia |
| $J_o$ | Other equivalent inertia |
| $J_s$ | Inertia of flywheel box |
| $J_{tup}, J_{tb}, J_{tf}, J_{tr}$ | Equivalent inertia of upper, lower, front, and rear parts of track |
| $l_d$ | Relative horizontal distance between centroid and geometric center |
| $m$ | Mass of whole vehicle |
| $m_v$ | Vehicle mass (excluding track) |
| $m_t$ | Mass of track |
| $m_{tup}, m_{tb}, m_{tf}, m_{tr}$ | Mass of upper, lower, front, and rear parts of track |
| $n_l$ | Number of load wheels |
| $n_b$ | Number of supporting rollers |
| $R$ | Effective radius of driving wheel |
| $R_1$ | Inner radius of load wheel |
| $R_2$ | Outer radius of load wheel |
| $s$ | Up (or down) slope distance |
| $t_i$ | Response time |
| $\Delta t$ | Sampling frequency(s) |
| $T$ | Road resistance moment |
| $T_{ti}$ | Driving torque in calibration |
| $T_a$ | Vehicle inertia torque |
| $T_{d1,d2}$ | Resistance in calibration |
| $T_e$ | Vehicle driving torque |
| $T_f$ | Ground resistance torque |
| $T_s$ | Slope resistance torque |
| $T_w$ | Wind resistance torque |
| $v_v$ | Vehicle speed |
| $v_t$ | Track speed |
| $v_{tup}, v_{tb}, v_{tf}, v_{tr}$ | Absolute speed of the upper, lower, front, and rear parts of the track |
| $v_{tupe}, v_{tbe}, v_{tfe}, v_{tre}$ | Traction velocity of the upper, lower, front, rear, front, and rear parts of the track |
| $v_{tupr}, v_{tbr}, v_{tfr}, v_{trr}$ | Relative velocity of upper, lower, front, and rear parts of the track to driving wheel |
| $\alpha_d$ | Angular acceleration of vehicle output axle |
| $\alpha_r$ | Measured acceleration |
| $\alpha_t$ | Target acceleration |
| $\alpha_i$ | Angular acceleration |

| | |
|---|---|
| $\gamma$ | Vehicle inclination |
| $\theta_i$ | Slope angle |
| $\omega_{em}$ | Target speed of driving wheel |
| $\omega$ | Measured speed of load simulation system |
| $\omega_l$ | Load wheel angular speed |
| $\omega_d$ | Driving wheel angular speed |
| $\omega_i$ | Angular speed of induced wheel |
| $\omega_b$ | Angular velocity of supporting roller |
| $\delta$ | Slip rate |
| $\xi$ | Sensor noise |
| $C(s)$ | Controller |
| $G(s)$ | Transfer function of motor |
| $G_n(s)$ | Nominal transfer function of load simulation system |
| $J(s)$ | Transfer function of transmission mechanism |
| $Q(s)$ | Filter |
| $\Delta(s)$ | Non-linear uncertainty |

## References


1. Wang, Z.; Lv, H.; Zhou, X.; Chen, Z.; Yang, Y. Design and Modeling of a Test Bench for Dual-Motor Electric Drive Tracked Vehicles Based on a Dynamic Load Emulation Method. *Sensors* **2018**, *18*, 1993. [CrossRef] [PubMed]
2. Takeda, M.; Hosoyamada, Y.; Motoi, N.; Kawamura, A. Development of the experiment platform for electric vehicles by using motor test bench with the same environment as the actual vehicle. In Proceedings of the IEEE International Workshop on Advanced Motion Control, Yokohama, Japan, 14–16 March 2014; pp. 356–361.
3. Hewson, C.R.; Sumner, M.; Asher, G.M.; Wheeler, P.W. Dynamic mechanical load emulation test facility to evaluate the performance of AC inverters. *Power Eng. J.* **2000**, *14*, 21–28. [CrossRef]
4. Hewson, C.R.; Asher, G.M.; Sumner, M.; Wheeler, P.W. Dynamic mechanical load emulation test facility to evaluate the performance of AC inverters. In Proceedings of the 7th International Conference on Power Electronics and Variable Speed Drives, London, UK, 21–23 September 1998; pp. 206–211.
5. Fu, W.X.; Sun, L.; Yu, Y.F.; Zhu, S.P.; Yan, J. Design and Model-building of Motor-driven Load Simulator with Large Torque Outputs. *J. Syst. Simul.* **2009**, *21*, 3596–3598.
6. Yalla, S.K.; Kareem, A.; Asce, M. Dynamic Load Simulator: Actuation Strategies and Applications. *J. Eng. Mech.* **2007**, *133*, 855–863. [CrossRef]
7. Tian, Y.; Jing, Z.; Wang, K.; Nie, S.; Lu, Q. *Study on the Control of AC Dynamometer System for Hybrid Electrical Vehicle Test Bench*; LTLGB 2012; Springer: Berlin/Heidelberg, Germany, 2013.
8. Rodic, M.; Jezernik, K.; Trlep, M. Dynamic emulation of mechanical loads: An advanced approach. *IEE Proc. Electr. Power Appl.* **2006**, *153*, 159–166. [CrossRef]
9. Fajri, P.; Ahmadi, R.; Ferdowsi, M. Test bench for emulating electric-drive vehicle systems using equivalent vehicle rotational inertia. In Proceedings of the IEEE Power & Energy Conference at Illinois, Champaign, IL, USA, 22–23 February 2013; pp. 83–87.
10. Huh, K.; Kim, J.; Hong, D. Estimation of dynamic track tension utilizing a simplified tracked vehicle model. In Proceedings of the American Control Conference, Arlington, VA, USA, 25–27 June 2001.
11. Kim, J.H.; Park, C.S.; Kim, S.G.; Kim, J.H. Hydraulic system design and vehicle dynamic modeling for the analysis and development of tire roller. *Int. J. Control Autom. Syst.* **2003**, *1*, 89–94.
12. Hewson, C.R.; Asher, G.M. Dynamometer control for emulation of mechanical loads. In Proceedings of the IEEE Industry Applications Conference, St. Louis, MO, USA, 12–15 October 1998; pp. 1511–1518.
13. Akpolat, Z.H.; Asher, G.M.; Clare, J.C. Experimental dynamometer emulation of nonlinear mechanical loads. *Ind. Appl. IEEE Trans.* **1999**, *35*, 1367–1373. [CrossRef]
14. Akpolat, Z.H.; Asher, G.M.; Clare, J.C. Dynamic emulation of mechanical loads using a vector- controlled induction motor-generator set. *Ind. Electron. IEEE Trans.* **1999**, *46*, 370–379. [CrossRef]

15. Rodic, M.; Jezernik, K.; Trlep, M. Use of dynamic emulation of mechanical loads in the testing of electrical vehicle driveline control algorithms. In Proceedings of the 2007 European Conference on Power Electronics and Applications, Aalborg, Denmark, 2–5 September 2007; pp. 1–10.
16. Kyslan, K.; Rodič, M.; Suchý, Ľ.; Ferková, Ž.; Ďurovský, F. Industrial controller-based dynamometer with dynamic emulation of mechanical loads. *Electr. Eng.* **2017**, *99*, 1245–1254. [CrossRef]
17. Kempf, C.J.; Kobayashi, S. Disturbance observer and feedforward design for a high-speed direct-drive positioning table. *Control Syst. Technol. IEEE Trans.* **1999**, *7*, 513–526. [CrossRef]
18. Gao, Y.; Sun, B.; Lu, G. Modified function projective lag synchronization of chaotic systems with disturbance estimations. *Appl. Math. Model.* **2013**, *37*, 4993–5000. [CrossRef]
19. Zhang, Z.; Wang, L.; Zhang, J.; Ma, R. Study on Requirements for Load Emulation of the Vehicle with an Electric Braking System. *IEEE Trans. Veh. Technol.* **2017**, *11*, 9638–9653. [CrossRef]
20. Li, W.L.; Wang, J.J.; Zhang, X.K.; Yi, P. A novel road dynamic simulation approach for vehicle driveline experiments. *Discret. Contin. Dyn. Syst.* **2019**, *12*, 1035–1052. [CrossRef]
21. Thompson, J.K.; Marks, A.; Rhode, D. Inertia Simulation in Brake Dynamometer Testing. In Proceedings of the SAE International, Brake Colloquium & Exhibition, Phoenix, AZ, USA, 6–9 October 2002.
22. Chou, H.H.; Kung, Y.S.; Quynh, N.V.; Cheng, S. Optimized FPGA design, verification and implementation of a neuro-fuzzy controller for PMSM drives. *Math. Comput. Simul.* **2013**, *90*, 28–44. [CrossRef]
23. Xing, Q.; Zhang, J.; Qian, M.; Jia, Z.; Sun, B. Design, calibration and error analysis of a piezoelectric thrust dynamometer for small thrust liquid pulsed rocket engines. *Measurement* **2011**, *44*, 338–344. [CrossRef]
24. Chavan, V.V.; Diggory, P.J.; Ulbrecht, I.J. Influence of dynamometer calibration on the accuracy of power consumption measurements. *Chem. Ing. Tech.* **1975**, *47*, 74. [CrossRef]
25. Meymand, S.Z.; Ahmadian, M. Design, Development, and calibration of a force-moment measurement system for wheel-rail contact mechanics in roller rigs. *Measurement* **2015**, *81*, 113–122. [CrossRef]
26. Yong, Y.; Xiao-jun, Z.; Chen-long, Y.; Jin-qiu, M. Dynamic distribution method of multi-axle vehicle's driving axle load on test bench. *J. Zhejiang Univ. Eng. Sci.* **2014**, *48*, 1080–1085.
27. Nam, Y. Dynamic characteristic analysis and force loop design for the aerodynamic load simulator. *J. Mech. Sci. Technol.* **2012**, *14*, 1358–1364. [CrossRef]
28. Chassin, F.S.; Mayhorn, E.T.; Elizondo, M.A.; Lu, S. Load modeling and calibration techniques for power system studies. In Proceedings of the 43th North American Power Symposium (NAPS), Boston, MA, USA, 4–6 August 2011.
29. Hong, W.; Qiang, S.; Shengbo, W.; Pu, Z. Dynamic modeling and control strategy optimization for a hybrid electric tracked vehicle. *Math. Probl. Eng.* **2015**, *2015*, 1–12.
30. Wang, H.; Sun, F.C. Dynamic Modeling and Simulation on a Hybrid Power System for Dual-Motor-Drive Electric Tracked Bulldozer. *Appl. Mech. Mater.* **2014**, *494–495*, 229–233. [CrossRef]
31. Fajri, P.; Ahmadi, R.; Ferdowsi, M. Equivalent vehicle rotational inertia used for electric vehicle test bench dynamic studies. In Proceedings of the Conference on IEEE Industrial Electronics Society, Montreal, QC, Canada, 25–28 October 2012.
32. Zou, Y.; Kong, Z.; Liu, T.; Liu, D. A Real-Time Markov Chain Driver Model for Tracked Vehicles and its Validation: Its Adaptability via Stochastic Dynamic Programming. *IEEE Trans. Veh. Technol.* **2016**. [CrossRef]
33. Fajri, P.; Lee, S.; Prabhala, V.A.K.; Ferdowsi, M. Modeling and Integration of Electric Vehicle Regenerative and Friction Braking for Motor/Dynamometer Test Bench Emulation. *IEEE Trans. Veh. Technol.* **2015**, *65*, 4264–4273. [CrossRef]
34. Carriere, S.; Caux, S.; Fadel, M. Optimised speed control in state space for PMSM direct drives. *IET Electr. Power Appl.* **2010**, *4*, 158–168. [CrossRef]
35. Cao, Y.Y.; Frank, P.M. Robust H disturbance attenuation for a class of uncertain discrete-time fuzzy systems. *IEEE Trans. Fuzzy Syst.* **2000**, *8*, 406–415.
36. Kim, M.S.; Shin, J.H.; Hong, S.G.; Lee, J.J. Designing a robust adaptive dynamic controller for nonholonomic mobile robots under modeling uncertainty and disturbances. *Mechatronics* **2003**, *13*, 507–519. [CrossRef]
37. Simon, D. *Optimal State Estimation: Kalman, H Infinity, and Nonlinear Approaches*; John Wiley & Sons: Hoboken, NJ, USA, 2006.
38. Wang, Z.; Ho, D.W.C.; Liu, Y.; Xiaohui, L. Robust H∞ H∞ mathContainer Loading Mathjax, control for a class of nonlinear discrete time-delay stochastic systems with missing measurements. *Automatica* **2009**, *45*, 684–691. [CrossRef]

39. Wang, T. Development and Calibration of an Item Response Model That Incorporates Response Time. *Appl. Psychol. Meas.* **2005**, *29*, 323–339. [CrossRef]
40. Wood, J.D. Calibration, Stability, and Response Time for Salinity Sensors. *Soil Sci. Soc. Am. J.* **1978**, *42*, 248–250. [CrossRef]
41. Vasilevskyi, O.M. Calibration method to assess the accuracy of measurement, devices using the theory of uncertainty. *Int. J. Metrol. Qual. Eng.* **2014**, *5*, 403. [CrossRef]

© 2019 by the authors. Licensee MDPI, Basel, Switzerland. This article is an open access article distributed under the terms and conditions of the Creative Commons Attribution (CC BY) license (http://creativecommons.org/licenses/by/4.0/).